AGU PUBLICATIONS

Radio Science

RESEARCH ARTICLE
10.1002/2016RS005959

Study of TEC fluctuation via stochastic models and Bayesian inversion

A. Bires[1,2], L. Roininen[3,4], B. Damtie[1], M. Nigussie[1], and H. Vanhamäki[2]

[1]Washera Geospace and Radar Science Laboratory, Bahir Dar University, Bahir Dar, Ethiopia, [2]Ionospheric Research Group, University of Oulu, Oulu, Finland, [3]Sodankylä Geophysical Observatory, University of Oulu, Sodankylä, Finland, [4]Department of Statistics, University of Warwick, Coventry, UK

Key Points:
- Change of the statistical parameters of the TEC time series
- Maximum a posteriori (MAP) estimation in Bayesian statistical inverse problems
- TEC fluctuation

Correspondence to:
A. Bires,
abiyot.workayehu@oulu.fi

Citation:
Bires, A., L. Roininen, B. Damtie, M. Nigussie, and H. Vanhamäki (2016), Study of TEC fluctuation via stochastic models and Bayesian inversion, *Radio Sci.*, *51*, 1772–1782, doi:10.1002/2016RS005959.

Received 21 JAN 2016
Accepted 5 OCT 2016
Accepted article online 28 OCT 2016
Published online 10 NOV 2016

Abstract We propose stochastic processes to be used to model the total electron content (TEC) observation. Based on this, we model the rate of change of TEC (ROT) variation during ionospheric quiet conditions with stationary processes. During ionospheric disturbed conditions, for example, when irregularity in ionospheric electron density distribution occurs, stationarity assumption over long time periods is no longer valid. In these cases, we make the parameter estimation for short time scales, during which we can assume stationarity. We show the relationship between the new method and commonly used TEC characterization parameters ROT and the ROT Index (ROTI). We construct our parametric model within the framework of Bayesian statistical inverse problems and hence give the solution as an a posteriori probability distribution. Bayesian framework allows us to model measurement errors systematically. Similarly, we mitigate variation of TEC due to factors which are not of ionospheric origin, like due to the motion of satellites relative to the receiver, by incorporating a priori knowledge in the Bayesian model. In practical computations, we draw the so-called maximum a posteriori estimates, which are our ROT and ROTI estimates, from the posterior distribution. Because the algorithm allows to estimate ROTI at each observation time, the estimator does not depend on the period of time for ROTI computation. We verify the method by analyzing TEC data recorded by GPS receiver located in Ethiopia (11.6°N, 37.4°E). The results indicate that the TEC fluctuations caused by the ionospheric irregularity can be effectively detected and quantified from the estimated ROT and ROTI values.

1. Introduction

The Global Positioning System (GPS) has been used as a remote sensing system for ionosphere by measuring Total Electron Content (TEC). The TEC, which is expressed in TEC unit (1 TECU = 10^{16} electrons per m^2), is defined as the integral of electron density along the GPS signal path from GPS satellites to the receiver. The method of probing the ionosphere remotely using the GPS system has become popular among the space physics community, because it is low cost and observation using a single GPS receiver can cover a wide ionospheric region.

One of the objectives of measuring TEC values using GPS receivers is to probe the irregularities in the ionospheric electron density that cause TEC fluctuations and radio signal scintillations. This can be done by characterizing the temporal variation of GPS TEC measurements. Mostly, the root-mean-square deviation of TEC (σ_{TEC}), ROT, and the standard deviation of ROT (ROTI) are used to characterize the TEC fluctuation. However, from the point of view of detecting TEC fluctuations due to ionospheric irregularity only, using ROT and ROTI are found to be advantageous over σ_{TEC}. This is because the algorithms to calculate ROT and ROTI are easily implemented, and taking the derivative of GPS TEC while computing ROT mitigates the effect of background trend [*Beach and Kintner*, 1999]. Despite the fact that calculating ROT is straightforward, differentiation may amplify the effects of glitches and measurement noise [*Beach and Kintner*, 1999; *Carrano and Groves*, 2007].

Recently, several studies have been done using ROTI to characterize the observed TEC fluctuations and to estimate the measure of the amplitude scintillation of radio wave (S_4) from the TEC fluctuation [e.g., *Pi et al.*, 1997; *Basu et al.*, 1999; *Beach and Kintner*, 1999; *Li et al.*, 2007; *Du et al.*, 2000; *Carrano and Groves*, 2007]. A comparison of S_4 with ROTI was made by *Pi et al.* [1997], *Basu et al.* [1999], *Beach and Kintner* [1999], and *Li et al.* [2007]. In these studies the algorithms implemented to calculate ROT and ROTI are the same, but the sample rate of the TEC data used and the time interval over which a value of ROTI is calculated vary among

some of the studies. In spite of these differences, all of the studies stated that the ROTI values could be used to identify the presence of ionospheric irregularities causing TEC fluctuation and signal scintillation.

In this paper, we model ROT as a continuous derivative of the time-sampled TEC data. For practical computations we discretize this model and cast the ROT estimation to the framework of Bayesian statistical inverse problems. In this way, we can freely choose the ROT sampling interval. For the estimation algorithm, we need to add some a priori information in order to obtain results when we have dense discretization. For this, we use Gaussian white noise prior. Given this approach, we can guarantee that the inverse problems reconstruction are essentially independent of TEC or ROT sampling interval.

Therefore, in this paper, we propose the maximum a posteriori (MAP) estimation technique in Bayesian statistical inverse problems to estimate ROT and ROTI. From the point of view of mitigating the effect of measurement noise, the MAP estimation approach is similar to estimation with regularization in classical approach, which is commonly used as an estimation technique for ill-posed problems. In classical regularization methods, mitigating the instability of the solution due to the measurement noise is done by introducing a slight modification of the original problem. When solving inverse problems using the framework of Bayesian probability theory, regularization of a problem is done by using prior information about the unknown random variable in the form of a probability distribution called the a priori distribution [e.g., *Roininen et al.*, 2011].

The rest of this paper is organized as follows: In section 2, we present methods for ROTI computation. Specifically, we remark the mathematical formula of the existing methods for ROT and ROTI computation. Subsection 2.1 describes the formulation of the proposed method for ROT and ROTI estimation. We first construct a linear stochastic measurement model that relates the realizations of TEC measurement with the random variables ROT. Then we construct the solution, i.e., the posterior distribution which consists of likelihood, a priori, and hyperprior distributions. We use optimization technique to find the MAP estimates of ROT and ROTI. Finally, in section 3 we demonstrate the new method by analyzing GPS TEC data recorded by a dual-frequency GPS receiver located at Bahir Dar (11.6°N, 37.4°E), Ethiopia.

2. Methodology

The rate of change of TEC (ROT) is defined as rate of change of TEC over the sampling time interval, and ROTI is defined as the standard deviation of the ROT over some time.

Traditionally, ROT (in TECU/min) is defined as [e.g., *Pi et al.*, 1997]

$$\mathrm{ROT}(t_j) = \frac{\mathrm{TEC}(t_j) - \mathrm{TEC}(t_{j-1})}{t_j - t_{j-1}}, \tag{1}$$

where t_j are the discrete TEC measurement times. ROTI is calculated over N successive ROT samples as [e.g., *Carrano and Groves*, 2007]

$$\mathrm{ROTI} = \sqrt{\langle \mathbf{ROT}^2 \rangle - \langle \mathbf{ROT} \rangle^2}, \tag{2}$$

where **ROT** is the vector of N successive ROT samples and $\langle \cdot \rangle$ denotes the mean. As mentioned in section 1, in the traditional approach the noise is enhanced by differentiation and ROTI values depend on calculation period of time. Therefore, we introduce a new method.

2.1. Stochastic Estimation of ROT and ROTI

We know that in practice all measurements are noisy. Hence, it is natural to model the measurements as stochastic processes. In this section, we construct a stochastic model for ROT and ROTI. Given the noisy TEC measurements, the solution of the Bayesian inverse problem; i.e., the a posteriori probability distribution is constructed. Then we consider how to draw estimators from the posterior distribution. The discretized TEC measurement is modelled in continuous time as

$$M(t) = \mathrm{TEC}(t) + E(t), \tag{3}$$

where $M(t)$, $\mathrm{TEC}(t)$, and $E(t)$ are the continuous-time noisy TEC measurements, unknown noiseless TEC, and E measurement noise, respectively. We are interested in studying the statistical properties of the rate of change of TEC. For the continuous-time measurement equation (1) is given by

$$\mathrm{ROT(t)} = \frac{\mathrm{d}}{\mathrm{d}t}\mathrm{TEC}(t). \tag{4}$$

We write this equation equivalently as

$$\mathrm{TEC}(t) = \int H(t - t')X(t')\mathrm{d}t', \tag{5}$$

where $H(t - t')$ is the Heaviside step function and $X(t') = \mathrm{ROT}(t')$. Substituting equation (5) into equation (3), the continuous-time measurement model becomes

$$M(t) = \int H(t - t')X(t')\mathrm{d}t' + E(t). \tag{6}$$

However, GPS TEC measurements are discrete. Thus, for a temporally sampled measurement we rewrite equation (6) as

$$M(t_j) = \int H(t_j - t')X(t')\mathrm{d}t' + E(t_j). \tag{7}$$

For numerical computation, we discretize the integral and obtain a matrix presentation

$$\mathbf{M} = A\mathbf{X} + \mathbf{E}, \tag{8}$$

where A is a known matrix, $\mathbf{M}$ is the measurement vector of observed GPS TEC values, $\mathbf{X}$ is the unknown vector of ROT values, and $\mathbf{E}$ is the measurement noise vector. In the Bayesian statistical inverse theory, all the variables included in the measurement model are considered as random variables. The degree of information concerning their realizations is coded in probability densities. Given the stochastic measurement model in equation (8), the task is to extract information about $\mathbf{X}$ from the measurements $\mathbf{M}$. This task of extracting information is called an inverse problem or a statistical inverse problem.

As the measurement model contains random variables, a natural framework for studying the inverse problem is probability theory. In this paper, we choose the Bayesian framework for statistical inverse problems to extract information about $\mathbf{X}$. This framework allows the extraction of information by inspecting the a posteriori probability distribution of the parameters $\mathbf{X}$, given the observed measurements $\mathbf{M}$.

The a posteriori distribution of the unknown parameters $\mathbf{X}$ conditioned on the measurements $\mathbf{M}$ is obtained by using Bayes's formula [e.g., *Doicu et al.*, 2010],

$$D_{\mathrm{ps}}(\mathbf{x}|\mathbf{m}) \propto D_{\mathrm{pr}}(\mathbf{x})D(\mathbf{m}|\mathbf{x}), \tag{9}$$

where the terms $D(\mathbf{m}|\mathbf{x})$ and $D_{\mathrm{pr}}(\mathbf{x})$, respectively, are called the likelihood and the a priori probability density. The a posteriori probability density $D_{\mathrm{ps}}(\mathbf{x}|\mathbf{m})$ contains all the information of the unknown random variables $\mathbf{X}$.

2.1.1. The Likelihood Density

The likelihood density $D(\mathbf{m}|\mathbf{x})$ is the probability density of the measurements, given the unknown parameters. The construction of the likelihood density depends on the noise $\mathbf{E}$ assumption [*Doicu et al.*, 2010]. In this paper, we model the measurement noise $\mathbf{E}$ by Gaussian density with zero-mean and known covariance matrix $\Gamma_e = \sigma^2\mathbf{I}$

$$\mathbf{E} \sim \mathcal{N}(\mathbf{0}, \sigma^2\mathbf{I}) \tag{10}$$

Assuming that $\mathbf{E}$ is independent of $\mathbf{X}$, the probability density $D(\mathbf{e})$ of it remains unchanged when conditioned on $\mathbf{X} = \mathbf{x}$. In this case, the measurements $\mathbf{M}$ conditioned on $\mathbf{X} = \mathbf{x}$ are distributed like $\mathbf{E}$ [*Doicu et al.*, 2010]. We write the likelihood density as

$$D(\mathbf{m}|\mathbf{x}) \propto \exp\left[-\frac{1}{2}(\mathbf{m} - \mathrm{A}\mathbf{x})^{\mathrm{T}}\Gamma_{\mathrm{e}}^{-1}(\mathbf{m} - \mathrm{A}\mathbf{x})\right]. \tag{11}$$

Given the measurements $\mathbf{M}$ and the measurement noise variance σ^2, we can extract information about the unknown variable $\mathbf{X}$ from likelihood density. Assuming that the density has only one strong peak, it is often practical to inspect the maxima of $D(\mathbf{m}|\mathbf{x})$, which is called the maximum likelihood (ML) estimate

$$\mathbf{x}_{\mathrm{ML}} = \arg\max_{\mathbf{x}} D(\mathbf{m}|\mathbf{x}). \tag{12}$$

Thus, $D(\mathbf{m}|\mathbf{x})$ has maximum at the point

$$\mathbf{x}_{\mathrm{ML}} = \left(A^T\Gamma_e^{-1}A\right)^{-1}A^T\Gamma_e^{-1}\mathbf{m}. \tag{13}$$

This is our first estimate of ROT which is computed without incorporating the a priori information. We can use this estimator when A is a square or overdetermined matrix and we have low noise. When the noise increases, and we have underdetermined A matrix, this estimator does not necessarily exist. If matrix $A \in \mathcal{R}^{j\times k}$ and $k > j$, then A is ill-posed and the problem has infinitely many solutions. In this case, unique solution can be found by regularizing the problem. In this study, we use our prior information about the unknown in the form of a priori probability density to regularize the problem. The construction of a priori probability density is presented in the next section.

2.1.2. A Priori Information

The TEC observations include a deterministic part (such as a trend due to motion of GPS satellites relative to GPS receivers on the ground) and a stochastic part due to the ionospheric variations. As suggested by *Zhang et al.* [2005], taking the higher-order (usually second-order) differences of TEC may reduce the deterministic part. This means that ROT which is defined from the first-order difference of TEC can also include both the deterministic and stochastic parts.

Based on this fact, we assume a priori that the random variable $\mathbf{X}$ is composed of a stochastic part and a deterministic part, and we write a stochastic model for it as

$$\mathbf{X} = \mathbf{X}_s + \mathbf{T}, \tag{14}$$

where $\mathbf{X}_s$ is a stochastic part and $\mathbf{T}$ is the deterministic part. We model the trend part by a two-sided moving average of $\mathbf{X}$, and the stochastic part is modeled as a Gaussian random process with zero expectation value.

Let z be a positive integer and consider the two-sided moving average,

$$\hat{\mathbf{T}}_t = \sum_{j=-z}^{j=z} a_j \mathbf{X}_{t-j}, \tag{15}$$

where $t = z+1, z+2, \ldots, n-z$ and a_j are the moving average weights. Assuming that $\mathbf{X}_t$ was generated by the process in equation (14) and that $\mathbf{T}_t$ is approximately linear over the interval $[t-z, t+z]$ and the average of the stochastic terms over this interval is zero, then $\mathbf{T}_t$ will be close to $\mathbf{T}_t$. Equation (15) can be interpreted as a low-pass filter since it takes $\mathbf{X}$ and removes from it the rapidly fluctuating (or high-frequency) component $\mathbf{X}_s$, and leaves the relatively slowly varying trend $\mathbf{T}_t$. The matrix representation of equation (15) is given by

$$\hat{\mathbf{T}} = P\mathbf{X}, \tag{16}$$

where $P \in \mathcal{R}^{n\times n}$ is a banded Toeplitz matrix which has the appearance of equation (17):

$$\mathrm{P} = \begin{bmatrix} a_0 & a_{-1} & \cdots & a_{-z} & & & & & & \\ a_1 & a_0 & & & & & & & & \\ \vdots & & & & & & & 0 & & \\ & & \ddots & & \ddots & & & & & \\ a_z & & & & & & & & & \\ & \ddots & & & & & & & & \\ & & a_z & \cdots & a_1 & a_0 & a_{-1} & \cdots & a_{-z} & \\ & & & & & & & & \ddots & \\ & & & & \ddots & & & & & a_{-z} \\ & 0 & & & & & & \ddots & & \vdots \\ & & & & & & & & a_0 & a_{-1} \\ & & & & & & a_z & \cdots & a_1 & a_0 \end{bmatrix}. \tag{17}$$

Now, the stochastic part is obtained by subtracting the estimated trend from X as

$$\mathbf{X} - \mathbf{T} \approx \mathbf{X}_s. \tag{18}$$

Substituting equation (16) into this, the model for the stochastic part becomes

$$\mathbf{X}_s = (\mathbf{I} - P)\mathbf{X} \equiv \tilde{P}\mathbf{X}. \tag{19}$$

When random disturbances of the ionospheric electron density happen, their effects on TEC will destroy the steady state of $\mathbf{X}_s$. During these kinds of circumstances, we model the stochastic parts $X_{s,j}$ by a Gaussian random process with zero expectation value

$$\mathbf{X}_{s,j} \sim \mathcal{N}(\mathbf{0}, \beta_j^2). \tag{20}$$

Assuming mutually independent random variables $\mathbf{X}_s$, the joint probability density of $\mathbf{X}_s$ conditioned the variance $\beta^2 = [\beta_1^2, \beta_2^2, \ldots, \beta_n^2]$ is given by

$$D(\mathbf{x}_s|\beta^2) = \frac{1}{(2\pi)^{\frac{n}{2}}|\Gamma_s|^{\frac{1}{2}}} \exp\left(-\frac{1}{2}\mathbf{x}_s^T\Gamma_s^{-1}\mathbf{x}_s\right), \tag{21}$$

where $\mathfrak{f}_s \in \mathcal{R}^{n\times n}$ is a diagonal covariance matrix given by

$$\mathfrak{f}_s = \begin{bmatrix} \beta_1^2 & 0 & 0 & \cdots & 0 \\ 0 & \beta_2^2 & 0 & \cdots & 0 \\ 0 & 0 & \beta_3^2 & \cdots & 0 \\ \vdots & \vdots & & \ddots & \vdots \\ 0 & 0 & \cdots & 0 & \beta_n^2 \end{bmatrix}. \tag{22}$$

Combining this and equation (19), we write a stochastic model as

$$\tilde{P}\mathbf{X} = \mathbf{X}_s, \%\mathbf{X}_s \sim \mathcal{N}(\mathbf{0}, \Gamma_s). \tag{23}$$

The joint a priori probability density of $\mathbf{X}$ conditioned the variance of $\mathbf{X}_s$ is given by

$$D(\mathbf{x}|\beta^2) = \frac{|\tilde{P}^T\Gamma_s^{-1}\tilde{P}|^{\frac{1}{2}}}{(2\pi)^{\frac{n}{2}}} \exp\left(-\frac{1}{2}\mathbf{x}^T\tilde{P}^T\Gamma_s^{-1}\tilde{P}\mathbf{x}\right), \tag{24}$$

where $|\bullet|$ stands for determinant operator. This a priori model accepts different rates of TECs ($\mathbf{X}_{s,j}$) which are assumed to be due to ionospheric activity. The value of the variance β_j^2 of $\mathbf{X}_{s,j}$, which is the same as ROTI_j^2, is a reflection of how large a rate of change we expect the stochastic part of TEC could have in the time interval $[t_{j-1}, t_j]$. A small value of β_j^2 may indicate undisturbed condition while a large value may indicate disturbed condition.

In equation (24), the a priori density of $\mathbf{X}$ depends on the variance of $\mathbf{X}_{s,j}$ and its estimate will contain both the deterministic and stochastic parts. However, our interest is to study the stochastic part which is assumed to be due to ionospheric activity. Hence, for this goal a priori density should be given in terms of $\mathbf{X}_s$. The immediate consequence of this observation is that, from the point of view of information, it does not make any difference whether we express the prior belief in terms of the $\mathbf{X}$ or in terms of its stochastic part $\mathbf{X}_s$. However, writing the $\mathbf{X}$ in terms of the $\mathbf{X}_s$ allows us to study the effect of ionospheric activity directly from the fluctuating component (=ROT). For this reason, we make the stochastic part $\mathbf{X}_s$ the unknowns of primary interest as explained below.

In equation (23) matrix $\tilde{P}$ is invertible and hence $\mathbf{X}_s$ can be transformed to $\mathbf{X}$ as

$$\mathbf{X} = \tilde{P}^{-1}\mathbf{X}_s = \tilde{B}\mathbf{X}_s, \tag{25}$$

where $\tilde{B} = \tilde{P}^{-1}$. Then, substituting equation (25) into equation (8), the stochastic measurement model becomes

$$\mathbf{M} = A\tilde{B}\mathbf{X}_s + \mathbf{E} = \tilde{A}\mathbf{X}_s + \mathbf{E}, \tag{26}$$

where $\tilde{A} = A\tilde{B}$. In this case the stochastic part $\mathbf{X}_s$ becomes the unknown of primary interest.

The next issue that we need to address is what we believed of the prior for the variances β_j^2 or ROTI that will be treated themselves as random variables. The construction of their probability density will be discussed in the next section.

2.1.3. A Hyperpriori Information

In equation (24), the a priori density $D_{pr}(\mathbf{x}_s)$ of $\mathbf{X}_s$ is conditioned on the variances β_j^2. These kinds of parameters which are used for describing the a priori density are also part of estimation. We consider the parameters β_j^2 as unknown parameters and include them in the estimation process. Therefore, we need to construct a probability distribution that conveys our prior beliefs about the parameters β_j^2. Commonly, the probability density model of the parameters is known as hierarchical or hyperpriori model [e.g., *Kaipio and Somersalo*, 2005].

The fact that $\mathbf{X}_s$ might contain some fluctuations with different magnitude leads us to choose a hyperprior that allows some of the β_j to deviate strongly from the average. A probability density that allows outliers can be the exponential distribution [*Calvetti and Somersalo*, 2007]. In this paper, an inverse gamma probability density is used as a hyperprior probability density. The hyperprior density is given by

$$D_{hp}(\beta) \propto \exp\left(-\frac{1}{\mu}\sum_{j=1}^{n}\frac{1}{\beta_j^2} - \frac{3}{2}\sum_{j=1}^{n}\ln\beta_j^2\right), \tag{27}$$

where $\mu > 0$, which is assumed to be fixed, is the center point of the hyperprior density. The joint prior probability density of $\mathbf{X}_s$ and β is

$$D(\mathbf{x}_s, \beta^2) = D_{pr}(\mathbf{x}_s|\beta^2)D_{hp}(\beta). \tag{28}$$

Substituting equations (24) and (27) into equation (28) gives

$$D\left(\mathbf{x}_s, \beta^2\right) \propto \exp\left(-\frac{1}{2}||\Gamma_s^{-\frac{1}{2}}\mathrm{x}_s||^2 + \ln|\Gamma_s^{-\frac{1}{2}}| - \frac{1}{\mu}\sum\nolimits_{j=1}^{n}\beta_j^{-2} - \frac{3}{2}\sum_{j=1}^{n}\ln\beta_j^2\right). \tag{29}$$

Now, we have two unknown random variables $\mathbf{X}_s$ and β^2 (ROT and ROTI, respectively) with their joint prior probability density given by equation (29). Thus, from the Bayes's formula it follows that the posterior distribution is of the form

$$D_{ps}(\mathbf{x}_s, \beta^2|\mathbf{m}) \propto D(\mathbf{m}|\mathbf{x}_s)D(\mathbf{x}_s, \beta^2). \tag{30}$$

2.1.4. The A Posteriori Density and MAP Estimate

The posterior distribution $D_{ps}(\mathbf{x}_s, \beta^2|\mathbf{m})$ defined by equation (30) is considered to be the complete solution of the inverse problem.

Substituting equations (11) and (29) into equation (30), the a posteriori distribution becomes

$$D_{ps}\left(\mathbf{x}_s, \beta^2|\mathbf{m}\right) \propto \exp\left(-\frac{1}{2}||\Gamma_e^{-\frac{1}{2}}\left(\mathbf{m} - \tilde{A}\mathbf{x}_s\right)||^2 - \frac{1}{2}||\mathrm{f}_s^{-\frac{1}{2}}\mathrm{x}_s||^2 - 2\sum_{j=1}^{n}\ln\beta_j^2 - \frac{1}{\mu}\sum_{j=1}^{n}\frac{1}{\beta_j^2}\right). \tag{31}$$

The knowledge of the a posteriori density in equation (31) gives information about $\mathbf{X}_s$ and β^2 (that is, ROT and ROTI) in terms of probability density. The probabilities encoded in $D_{ps}(\mathbf{x}_s, \beta^2|\mathbf{m})$ are difficult to visualize; however, since both $\mathbf{X}_s$ and β^2 ranges in n-dimensional space, it is possible to compute some point estimates from the posterior density. A popular point estimator is the maximum a posteriori (MAP) estimator

$$\left(\mathbf{x}_{s,\mathrm{map}}, \boldsymbol{\beta}_{\mathrm{map}}^2\right) = \arg\max_{(\mathbf{x}_s,\beta^2)} D_{ps}(\mathbf{x}_s, \beta^2|\mathbf{m}). \tag{32}$$

We found the MAP estimates for $\mathbf{X}_s$ and β^2 by alternatingly maximizing the a posteriori distribution as described in Appendix A.

3. Results

The method described in the previous section has been demonstrated by analyzing TEC data obtained on 1 February 2008 and 13 April 2012 from a GPS station found in Bahir Dar (11.6°N, 37.4°E), Ethiopia. The TEC and S_4 data used in this paper are computed over each minute interval from dual-frequency GPS receiver observables using the standard methods described by, e.g., *Carrano and Groves* [2007b].

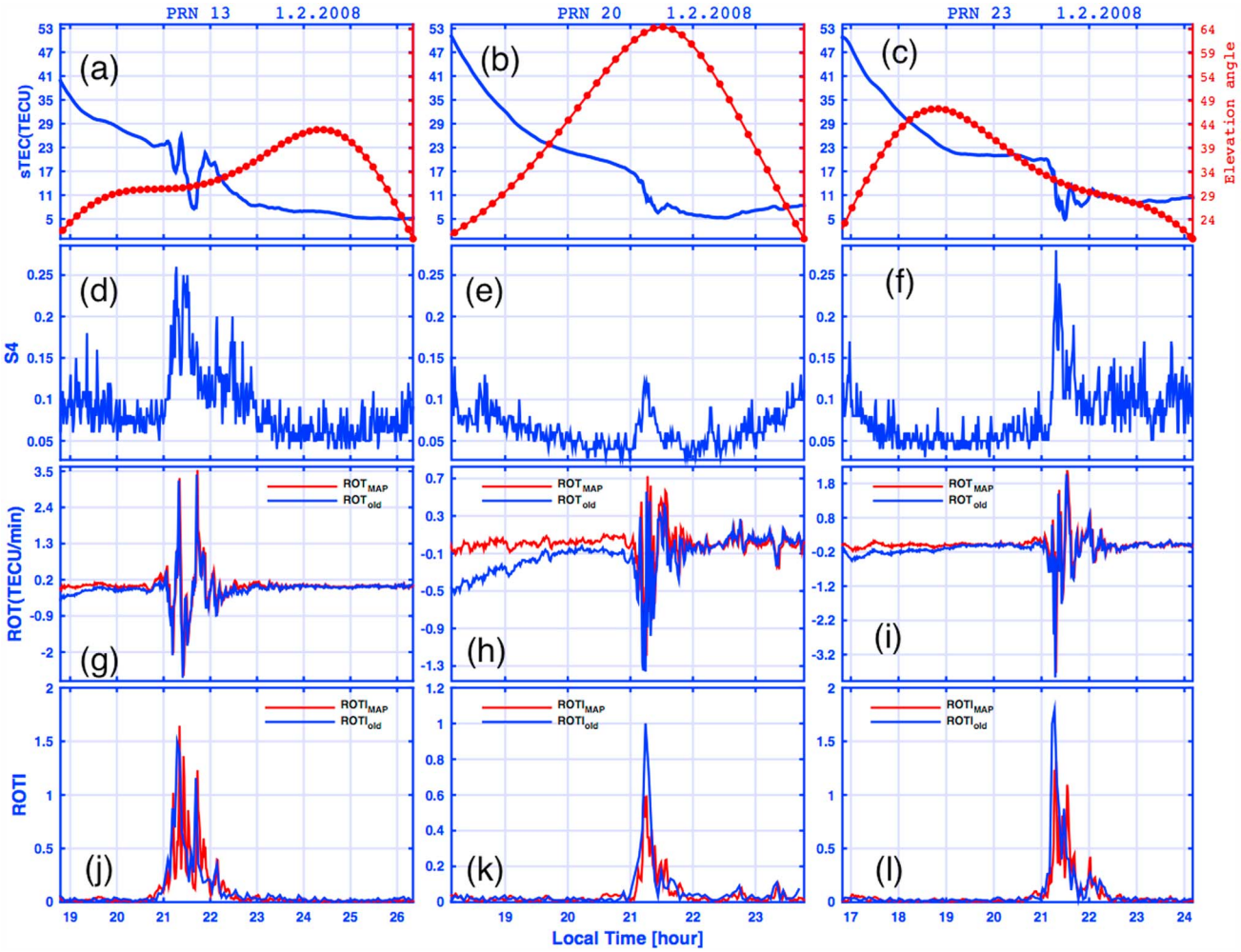

Figure 1. The Local Time variation of elevation angle, slant TEC (sTEC), S4 index, ROT, and ROTI on 1 Februar2008 from three GPS satellites (PRNs), (a, d, g, and j) PRN 13, (b, e, h, and k) PRN 20, and (c, f, i, and l) PRN 23. The curves of ROT_{old} and ROT_{MAP} (Figures 1g, 1h, and 1i) are calculated using the old method and the new method, respectively. The ROTI values calculated using the traditional method ($ROTI_{old}$) and the new method ($ROTI_{MAP}$) are shown on Figures 1j, 1k, and 1l. Local Time (LT) = Universal Time (UT) + 3, 1 TECU = 10^{16} el m^{-2}.

Figures 1 and 2 show the Local Time (LT) variations of TEC, satellite elevation angle, S_4 index, ROT, and ROTI from three GPS satellites each (Figure 1: PRNs 13, 20, and 23, and Figure 2: PRNs 15, 26, and 27). In Figures 1a, 1b, and 1c the blue smooth curve is for the measured TEC values and the red dotted curve is for elevation angles of the GPS satellites. The values of measured TEC and elevation angles, respectively, are shown on the left and right vertical axes. Both Figures 1d–1f, 1g–1i, and 1j–1l and Figures 2d–2f, 2g–2i, and 2j–2l show the time variation of S_4, ROT, and ROTI, respectively.

Rapid fluctuations in TEC are clearly seen in both figures. In Figure 1, the irregularity in the ionospheric electron density causes fluctuation of the TEC values (Figures 1a–1c between 21:00 and 22:30 LT, between 21:00 and 22:30 LT, and between 21:00 and 22:30 LT, respectively) and increase in the values of S_4 (Figures 1d–1f) between 21:00 and 22:30 LT, between 21:00 and 22:00 LT, and between 21:00 and 22:30 LT, respectively) when a bubble passes between the receiver and the satellite. Similarly, in Figure 2 the effect of ionospheric irregularity on TEC is clearly seen on ROT values (Figures 2g–2i) and ROTI values (Figures 2j–2l). This variation is accompanied with an increase in the values of S_4.

The S_4 enhancement seen simultaneously with the TEC fluctuation suggests the coexistence of ionospheric irregularities causing phase and amplitude scintillations. In Figure 1, the S_4 has two noticeable peaks in the line of sight of PRN 13 and PRN 23 (correspond to the patch of the ionospheric irregularity which has two

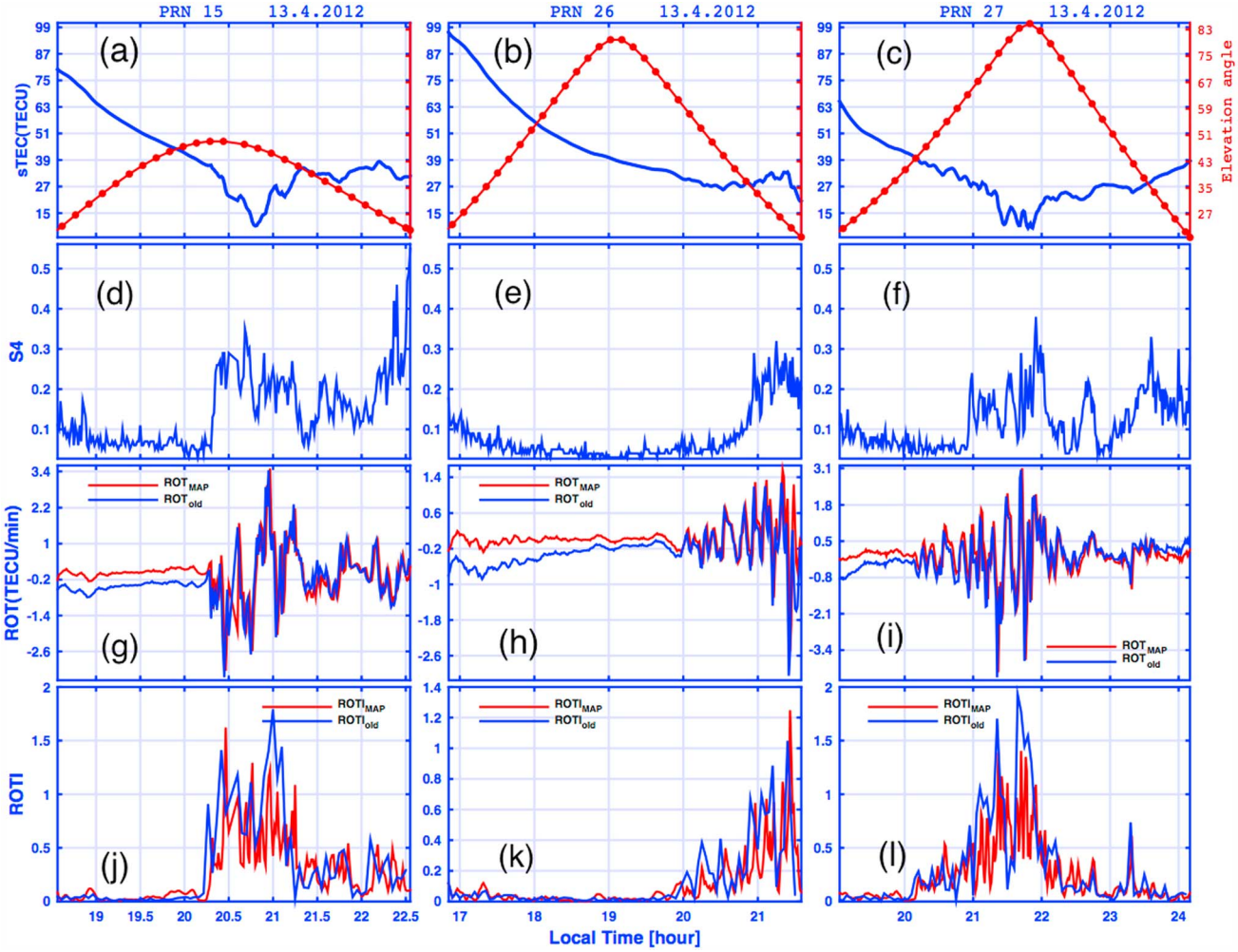

Figure 2. Same as Figure 1 but with data observed on 13 April 2012 using satellites PRN 15, 26, and 27.

noticeable scintillating regions in the line of sight of PRN 13 and PRN 23), and a single S_4 peak (one scintillating region) is seen in the line of sight of PRN 20. In Figure 2, the S_4 has more than two noticeable peaks in the line of sight of PRN 15 and PRN 27 (correspond to the patch of the ionospheric irregularity which has more than two noticeable scintillating regions in the line of sight of PRN 15 and PRN 27), and a single S_4 peak (one scintillating region) is seen in the line of sight of PRN 26. In particular, the S_4 value of PRN 15 shows significant enhancement in between 22 and 22:30 LT. But during this time the effect on TEC is not that pronounced (as seen from ROT and ROTI values). This suggests the presence of ionospheric irregularities that cause signal amplitude scintillation without affecting the phase.

Figures 1g–1i and 2g–2i show the local time variation of ROT computed at each minute interval. Here the two curves, ROT_{old} and ROT_{MAP}, correspond to estimates using the old method and new method or equations (1) and (A9), respectively. It is clearly seen that both ROT_{old} and ROT_{MAP} capture fluctuation in TEC and the S_4 enhancement. However, the background trend imposed by the solar zenith angle and satellite elevation angle variation is seen as a linear increase in the ROT_{old} values only (in Figure 1, between 19:00 and 20:00 LT for PRN 13, between ≈18:30 and 21:00 LT for PRN 20, and between 17:00 and 19:00 LT for PRN 23, and in Figure 2, 20:10–21:10 LT for PRN 15, 20:00–21:40 LT for PRN 26, and 20:10–22:20 LT for PRN 27). The results show that the new method effectively eliminates deterministic component in the estimated ROT_{MAP} values.

Figures 1j–1l and 2j–2l show local time variation of ROTI. The $ROTI_{old}$ and $ROTI_{MAP}$, respectively, are calculated using the old and new methods or equations (2) and (A7). The $ROTI_{MAP}$ is estimated at each minute interval using the new method while the $ROTI_{old}$ values are calculated at 3 min interval using the traditional method. The $ROTI_{old}$ values depicted in this figure capture only the major fluctuation structures seen on the TEC and S_4

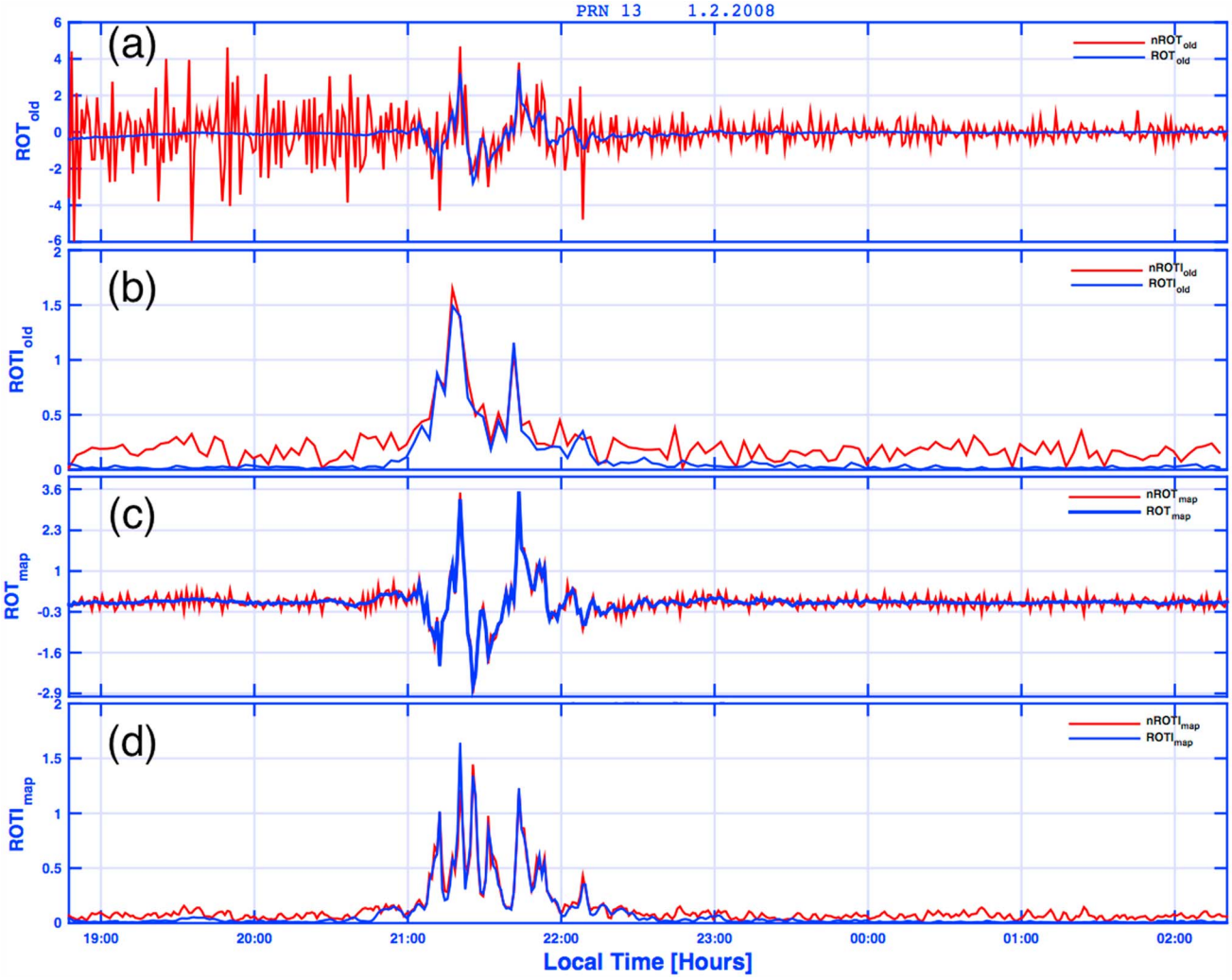

Figure 3. Comparison of ROT and ROTI values calculated from both noisy and noiseless TEC measurements. The curves of (a) ROT_{old} and (c) ROT_{map} are calculated using the old method and the new method, respectively. The ROTI values calculated using the (b) existing method ($ROTI_{old}$) and (c) the new method ($ROTI_{map}$) are shown. In all panels the red curves ($nROT_{old}$, $nROT_{map}$, $nROTI_{old}$, and $nROTI_{map}$) and blue curves (ROT_{old}, ROT_{map}, $ROTI_{old}$, and $ROTI_{map}$) represent results from TEC with noise and without noise, respectively.

data, while the $ROTI_{MAP}$ values capture both the fine and major fluctuations. The magnitude of $ROTI_{MAP}$ values have shown difference among the satellites. At the time where there is an irregularity which causes both TEC oscillation and amplitude scintillation, the ratio of ROTI to S_4 values are related to the phase scintillation index. In this study, we calculate the ratio $ROTI_{MAP}/S_4$ and $ROTI_{old}/S_4$ for each satellite. The ratio is calculated by taking the maximum of ROTI and S_4 values. For the event on 1 February 2008 we found $ROTI_{MAP}/S_4 \approx 5.9, 5.4, 5.0$, and $ROTI_{old}/S_4 \approx 5.8, 8.3$, and 6.4 for PRNs 13, 20, and 23, respectively. In the same way for the event on day 13 April 2012, $ROTI_{MAP}/S_4 \approx 4.9, 4.2, 3.7$, and $ROTI_{old}/S_4 \approx 5.1, 3.1$, and 5 for PRNs 13, 20, and 23, respectively. The magnitude of the S_4 values measured by the six satellites lies between 0.12 and 0.38. For these ranges of S_4 values, the corresponding $ROTI_{MAP}/S_4$ varies between 3.7 and 6.2, and $ROTI_{old}/S_4$ lies between 3.1 and 8.3. The narrow range of the ratio $ROTI_{MAP}/S_4$ is more consistent to the range of S_4 values, indicating that the new method captures the variations more reliably than the standard $ROTI_{old}$ estimate.

Finally, we have demonstrated the effect of noisy measurement on the estimates of both the new and old methods in Figure 3. As a noisy measurement, we use the TEC measurement with additive random noise having constant variance of magnitude equal to 1% of the maximum of error-free TEC. From this noisy TEC, both ROT and ROTI values are calculated using both the new ($nROT_{map}$ and $nROTI_{map}$) and old ($nROT_{old}$ and $nROTI_{old}$). The $nROT_{map}$ and $nROTI_{map}$ values are estimated using white noise prior with constant variance $\sigma_e^2\mathbf{I}$. Figures 3a and 3b show ROT and ROTI values estimated using the old method. It is clearly seen that there is

significant difference among estimates from noisy TEC and noiseless TEC, i.e, between $nROT_{old}$ and ROT_{old}, and between $nROTI_{old}$ and $ROTI_{old}$. Figures 3c and 3d, respectively, show ROT and ROTI values estimated using the new method. The MAP estimators look essentially the same for both noisy and noiseless measurements.

4. Conclusion

The change of state of the ionosphere from its quiet to disturbed conditions is reflected in the *F* region electron density and leads to changes in the statistical parameters of the TEC time series. This means that if accurately estimated, values of the statistical parameters of the ionospheric TEC can be used to monitor and quantify ionospheric activity in real time. Monitoring and detecting the ionospheric disturbances is important for prediction of the space weather, GPS surveying, and satellite navigation and communication.

In this paper, we have presented an improved method for the computation of ROT and ROTI based on maximum a posteriori (MAP) estimation in Bayesian statistical inverse problems. The new method provides a powerful and convenient way of mitigating the effect of a slowly varying background trend and measurement noise by incorporating a priori information in the form of probability density. The new method is demonstrated by analyzing the dual-frequency GPS TEC data from a receiver in Bahir Dar during 2 days. The results indicate that the estimated ROT_{MAP} and $ROTI_{MAP}$ values capture both the major and fine fluctuation structures in the TEC and S_4 better than the traditional estimates. Most importantly, the new method is better than the old method in controlling the effect of measurement noise on the estimates. The result also shows that the estimates are free from the effects imposed by variations of satellite elevation and solar zenith angles.

Appendix A: Optimization Steps

The joint a posteriori distribution of $\mathbf{X}_s$ and β^2 conditioned on the realizations of the measurement vector $\mathbf{M}$ is

$$D_{ps}(\mathbf{x}_s, \beta^2|\mathbf{m}) \propto \exp(-F(\mathbf{x}_s, \beta^2), \tag{A1}$$

where the function $F(\mathbf{x}_s, \beta^2)$ is defined by

$$F\left(\mathbf{x}_s, \beta^2\right) = \frac{1}{2}\left\|\begin{bmatrix}\Gamma_e^{-\frac{1}{2}}\tilde{A}\\ \Gamma_s^{-\frac{1}{2}}\end{bmatrix}\mathbf{x}_s - \begin{bmatrix}\Gamma_e^{-\frac{1}{2}}\mathbf{m}\\ \mathbf{0}\end{bmatrix}\right\|^2 + \frac{1}{\mu}\sum_{j=1}^{n}\beta_j^{-2} + 2\sum_{j=1}^{n}\ln\beta_j^2. \tag{A2}$$

The MAP estimates for $\mathbf{X}_s$ and β^2 can also be found by minimizing the functional $F(\mathbf{x}_s, \beta^2)$ as

$$\left(\mathbf{x}_{s,map}, \beta^2_{map}\right) = \arg\min_{(\mathbf{x}_s, \beta^2)} F(\mathbf{x}_s, \beta^2). \tag{A3}$$

In this paper, the MAP estimates for the pair $(\mathbf{X}_s, \beta^2)$ are computed by solving two minimization problems alternatingly. The scheme for computation is briefly described as follows:

1. *Initialize the value of* μ. As initial point for the estimation, begin by initializing μ. As shown in equation (A6), $\frac{1}{\mu}$ bounds β^2_{map} from below. Therefore, the initial value of μ should be set to make the initial values of β^2 a minimum (that is normal ionospheric condition).
2. *Estimate* $\mathbf{X}_{s,map}$. The MAP estimate of $\mathbf{X}_s$ is the minimizer of $F(\mathbf{x}_s, \beta^2)$ conditioned on $\beta^2 = \frac{1}{\mu}[1, 1, \ldots, 1]^T$. This means that the value of $\mathbf{x}_{s,map}$ is the solution of the equation $\nabla_{\mathbf{x}_s} F(\mathbf{x}_s, \beta^2) = 0$, that is,

$$\mathbf{x}_{s,map} = \left(\tilde{A}^T\Gamma_e^{-1}\tilde{A} + \Gamma_s^{-1}\right)^{-1}\tilde{A}^T\Gamma_e^{-1}\mathbf{m}. \tag{A4}$$

3. *Estimate* $\boldsymbol{\beta}^2_{map}$. Having the $\mathbf{x}_{s,map}$ values, the $\boldsymbol{\beta}^2_{map}$ is obtained by minimizing the function $F(\mathbf{x}_s, \beta^2)$ conditioned on $\mathbf{x}_{s,map}$. The current value of β^2 is the solution of equation

$$\nabla_{\beta^2_\lambda} F\left(\mathbf{x}_{s,map}, \beta^2\right) = 0. \tag{A5}$$

We found a formula for the solution

$$\boldsymbol{\beta}^2_{map,c} = \frac{1}{2\mu}\mathbf{U} + \frac{1}{4}||\left(\tilde{A}^T\Gamma_e^{-1}\tilde{A} + \Gamma_s^{-1}\right)^{-1}\tilde{A}^T\Gamma_e^{-1}\mathbf{m}||^2 \tag{A6}$$

and

$$\mathrm{ROTI}_{\mathrm{map}} = \left[\frac{1}{2\mu}\mathbf{U} + \frac{1}{4}||\left(\tilde{\mathrm{A}}^{\mathrm{T}}\Gamma_e^{-1}\tilde{\mathrm{A}} + \Gamma_{\mathrm{s}}^{-1}\right)^{-1}\tilde{\mathrm{A}}^{\mathrm{T}}\Gamma_e^{-1}\mathbf{m}||^2\right]^{\frac{1}{2}}, \tag{A7}$$

where $\mathbf{U} \in \mathcal{R}^n$ is a vector with $\mathbf{U}(j,1) = 1, 1 \le j \le n$. The diagonal covariance matrix Γ_{s} is updated as

$$\mathbf{\Gamma}_{\mathrm{s,map}} = \mathrm{diag}\left(\beta^2_{\mathrm{map,c}}\right). \tag{A8}$$

4. *Update* $\mathbf{x}_{\mathrm{s,map}}$. Having the current MAP estimate $\boldsymbol{\beta}^2_{\mathrm{map,c}}$, the $\mathbf{x}_{\mathrm{s,map}}$ is updated by using the formula

$$\mathbf{x}_{\mathrm{s,map}} = \left(\tilde{\mathrm{A}}^{\mathrm{T}}\Gamma_e^{-1}\tilde{\mathrm{A}} + \Gamma^{-1}_{\mathrm{s,map}}\right)^{-1}\tilde{\mathrm{A}}^{\mathrm{T}}\Gamma_e^{-1}\mathbf{m}. \tag{A9}$$

At this step, first reconstruct TEC ($\mathrm{TEC}_{\mathrm{rec}}$) by using the formula

$$\mathrm{TEC}_{\mathrm{rec}} = \tilde{\mathrm{A}}\mathbf{x}_{\mathrm{s,map}} \tag{A10}$$

and then calculate the root-mean-square error (RMSE) between the $\mathrm{TEC}_{\mathrm{rec}}$ and the observed TEC ($\mathrm{TEC}_{\mathrm{obs}}$) values via

$$\mathrm{RMSE} = \sqrt{\frac{1}{n}\sum_{j=1}^{n}\left(\mathrm{TEC}_{\mathrm{obs}}(t_j) - \mathrm{TEC}_{\mathrm{rec}}(t_j)\right)^2}. \tag{A11}$$

We allow the total number of iteration steps to reduce the RMSE value below a tolerance value of 10^{-3}. If this criteria is not met, repeat steps 3 and 4.

Acknowledgments
This work has been funded by the American Air Force Office of Scientific Researches (AFOSR), USA, under the project *Understanding the unique characteristics of equatorial ionosphere* (FA8655-13-1-3052), and Academy of Finland (application 250215, Finnish Program for Centers of Excellence in Research 2012–2017), Ministry for Foreign Affairs of Finland (HEI-ICI project HELM406-10), and Center for International Mobility of Finland (North-South project East-Africa Techno mathematics IV 2013–2015 project 2013-NSS-1). The data used for demonstration is obtained from Washera Geospace and Radar Science Laboratory, Bahirdar, Ethiopia: Contact person: Melessew Nigussie (melessewnigussie@yahoo.com).

References

Basu, S., K. M. Groves, J. M. Quinn, and P. Doherty (1999), A comparison of TEC fluctuation and scintillations at Ascension Island, *J. Atmos. Sol. Terr. Phys.*, *61*, 1219–1226.

Beach, T. L., and P. M. Kintner (1999), Simultaneous global position system observations of equatorial scintillations and total electron content fluctuations, *J. Geophys. Res.*, *104*, 22,553–22,565.

Calvetti, D., and E. Somersalo (2007), *Introduction to Bayesian Scientific Computing: Ten Lectures on Subjective Computing*, Springer Science+Business Media, LLC, New York.

Kaipio, J. P., and E. Somersalo (2005), *Statistical and Computational Inverse Problems*, Dordrecht, Springer Science+Business Media, Inc.

Carrano, C. S., and K. M. Groves (2007), TEC gradients and fluctuations at low latitudes measured with high data rate GPS receivers, in *Proceedings of the 63rd Annual Meeting of The Institute of Navigation (2007)*, pp. 156–163, Cambridge, Mass., 23–25 April.

Carrano, C. S., and K. M. Groves (2007b), *Ionospheric Monitoring with SCINDA*, IHY-AFRICA Space Weather Science and Education Workshop, Addis Ababa, Ethiopia.

Doicu, A., T. Trautmann, and F. Schreier (2010), *Numerical Regularization for Atmospheric Inverse Problems*, Springer, Berlin.

Du, J., P. Wilkinson, R. Thomas, and M. Cervera (2000), Determination of equatorial ionospheric scintillation S_4 by dual frequency GPS, URSI Commission G, Workshop, La Trobe University, Australia.

Li, G., B. Ning, and H. Yuan (2007), Analysis of ionospheric scintillation spectra and TEC in the Chinese low latitude region, *Earth Planets Space*, *59*(193), 259–285.

Pi, X., A. J. Mannucci, U. J. Lindqwister, and C. M. Ho (1997), Monitoring of global ionospheric irregularities using the worldwide GPS network, *Geophys. Res. Let.*, *24*(18), 2282–2286.

Roininen, L., M. S. Lehtinen, S. Lasanen, M. Orispää, and M. Markkanenm (2011), Correlation priors, *Inverse Prob. Imag.*, *5*, 167–184.

Zhang, H., J. Wang, W. Y. Zhu, and C. Huang (2005), Gaussian random process and its application for detecting the ionospheric disturbances using GPS, *J. Global Position Syst.*, *4*(1–2), 76–81.